

1-1-2012

Dye regeneration and charge recombination in dye-sensitized solar cells with ferrocene derivatives as redox mediators

Torben Daeneke
Monash University

Attila J. Mozer
University of Wollongong, attila@uow.edu.au


Tae-Hyuk Kwon
University of Melbourne

Noel W. Duffy
CSIRO

Andrew B. Holmes
University of Melbourne

See next page for additional authors

Follow this and additional works at: <https://ro.uow.edu.au/scipapers>

 Part of the [Life Sciences Commons](#), [Physical Sciences and Mathematics Commons](#), and the [Social and Behavioral Sciences Commons](#)

Recommended Citation

Daeneke, Torben; Mozer, Attila J.; Kwon, Tae-Hyuk; Duffy, Noel W.; Holmes, Andrew B.; Bach, Udo; and Spiccia, Leone: Dye regeneration and charge recombination in dye-sensitized solar cells with ferrocene derivatives as redox mediators 2012, 7090-7099.
<https://ro.uow.edu.au/scipapers/4263>

Dye regeneration and charge recombination in dye-sensitized solar cells with ferrocene derivatives as redox mediators

Abstract

Ferrocene compounds are promising redox shuttles for application in dye-sensitized solar cells (DSCs). Chemical modification of the cyclopentadienyl rings is easily achievable affording almost unlimited variation of the redox properties. This allows fine-tuning of the driving force for dye-regeneration and optimization of the energy conversion efficiency of DSCs. Herein, six ferrocene derivatives have been chosen for investigation which cover the large redox potential range of 0.85 V, by virtue of simple alkylation and halogenation of the cyclopentadienyl ring, and enable improved matching of the energy levels of the sensitizer and the electrolyte. Although the focus of this work was to examine the effect of the redox potential on charge transfer processes, DSCs were fabricated which achieved high energy conversion efficiencies of over 5%. Charge transfer reactions were studied to reveal the dependence of the dye regeneration rate, recombination losses and recombination pathways on the reaction driving force. An increase in redox potential led to a higher efficiency due to higher open circuit potentials until a threshold is reached. At this threshold, the driving force for dye regeneration ($18 \text{ kJ DE}^{-1} \approx 0.19 \text{ V}$) becomes too small for efficient device operation, leading to rapid recombination between the oxidized dye and electrons in the TiO₂ conduction band. As a result of this work guidelines can be formulated to aid the selection of redox couples for a particular sensitizer in order to maximize the utilization of incident solar energy.

Keywords

mediators, charge, ferrocene, regeneration, dye, cells, derivatives, solar, sensitized, redox, recombination

Disciplines

Life Sciences | Physical Sciences and Mathematics | Social and Behavioral Sciences

Publication Details

Daeneke, T., Mozer, A. J., Kwon, T., Duffy, N. W., Holmes, A. B., Bach, U. & Spiccia, L. (2012). Dye regeneration and charge recombination in dye-sensitized solar cells with ferrocene derivatives as redox mediators. *Energy and Environmental Science*, 5 (5), 7090-7099.

Authors

Torben Daeneke, Attila J. Mozer, Tae-Hyuk Kwon, Noel W. Duffy, Andrew B. Holmes, Udo Bach, and Leone Spiccia

Dye regeneration and charge recombination in dye-sensitized solar cells with ferrocene derivatives as redox mediators†

Torben Daeneke,^a Attila J. Mozer,^b Tae-Hyuk Kwon,^c Noel W. Duffy,^d Andrew B. Holmes,^c Udo Bach^{*e} and Leone Spiccia^{*a}

Received 2nd February 2012, Accepted 28th February 2012

DOI: 10.1039/c2ee21257a

Ferrocene compounds are promising redox shuttles for application in dye-sensitized solar cells (DSCs). Chemical modification of the cyclopentadienyl rings is easily achievable affording almost unlimited variation of the redox properties. This allows fine-tuning of the driving force for dye-regeneration and optimization of the energy conversion efficiency of DSCs. Herein, six ferrocene derivatives have been chosen for investigation which cover the large redox potential range of 0.85 V, by virtue of simple alkylation and halogenation of the cyclopentadienyl ring, and enable improved matching of the energy levels of the sensitizer and the electrolyte. Although the focus of this work was to examine the effect of the redox potential on charge transfer processes, DSCs were fabricated which achieved high energy conversion efficiencies of over 5%. Charge transfer reactions were studied to reveal the dependence of the dye regeneration rate, recombination losses and recombination pathways on the reaction driving force. An increase in redox potential led to a higher efficiency due to higher open circuit potentials until a threshold is reached. At this threshold, the driving force for dye regeneration (18 kJ mol^{-1} , $\Delta E = 0.19 \text{ V}$) becomes too small for efficient device operation, leading to rapid recombination between the oxidized dye and electrons in the TiO_2 conduction band. As a result of this work guidelines can be formulated to aid the selection of redox couples for a particular sensitizer in order to maximize the utilization of incident solar energy.

^aSchool of Chemistry, ARC Centre of Excellence for Electromaterials Science, Monash University, Victoria 3800, Australia. E-mail: Leone.Spiccia@Monash.edu; Fax: +61 3 99054597; Tel: +61 3 9905 4526

^bIntelligent Polymer Research Institute, ARC Centre for Excellence for Electromaterials Science, University of Wollongong, Wollongong, 2522, Australia

^cSchool of Chemistry, Bio21 Institute, University of Melbourne, Victoria 3010, Australia

^dCSIRO Energy Technology, Clayton, VIC 3169, Australia

^eDepartment of Materials Engineering, Monash University, Victoria 3800, Australia. E-mail: Udo.Bach@Monash.edu

† Electronic supplementary information (ESI) available: Elemental analysis (SI-T1), cyclic voltammetry data of the ferrocene derivatives in benzonitrile and acetonitrile (SI-T2 and T3), tabulated $J-V$ results (SI-T4), additional transient absorption data (SI-F1 and SI-T5), IMVS data (SI-F2) and charge extraction data (SI-F3 to F8). See DOI: 10.1039/c2ee21257a

Broader context

Dye-sensitized solar cells (DSCs) are intensively investigated as an alternative energy source to move modern society away from fossil fuels to a more sustainable economy based on renewable energy. While DSCs can be easily manufactured from abundant materials, resulting in low production costs, the redox active electrolyte represents a major drawback. Researchers in the field have recently intensified efforts to replace the common but highly corrosive iodide/triiodide based electrolytes with more suitable alternatives. At present, however, relatively little is known on how changes in the electrolyte, especially the redox potential of the redox couple, will affect DSC performance. This work is founded on our recent report of highly efficient DSCs utilizing the ferrocene/ferrocenium redox couple. Simple modifications of the cyclopentadienyl ligand in these compounds allow us to tune the redox potential of the electrolyte and to study the device performance and underlying charge transfer reactions in detail. We report an investigation of dye regeneration and recombination reactions together with their dependence on electrolyte potential and available driving force. Our findings are used to make recommendations aiding efforts to match a particular sensitizer with a suitable redox couple.

Introduction

In dye-sensitized solar cells (DSCs), light absorption by a dye adsorbed onto a mesoporous wide bandgap semiconductor film results in electron injection into the semiconductor conduction band.¹ A redox couple present in the electrolyte regenerates (reduces) the photo-oxidized dye and facilitates charge transport between the photoanode and cathode (Fig. 1). Device optimization, primarily focusing on the sensitizer, semiconductor and electrolyte, has resulted in efficiencies exceeding 12%.^{2–5} Until recently, the highest efficiencies have been reported for ruthenium(II) polypyridyl complexes.^{2,3,6–9} Metalloporphyrin and organic sensitizers, on the other hand,^{10–15} have achieved DSC efficiencies of up to 11%. Co-sensitization, utilizing more than one dye, has proven useful for optimizing light absorption to achieve panchromatic light harvesting.^{14,16,17} In fact, the recently reported 12.3% efficiency at full sunlight was achieved by co-sensitization of TiO₂ with a porphyrin and an organic dye while using a tris(2,2'-bipyridyl)cobalt(II/III) based redox electrolyte.⁵

The redox mediator in the electrolyte plays the important role of shuttling electrons from the cathode to the photoanode, where it regenerates the photo-oxidized dye in order for energy conversion to continue. Many types of electrolytes have been developed for use in DSCs, employing organic solvents, ionic liquids,^{18,19} plastic crystals²⁰ and solidifying agents.²¹ The primary objectives have been to reduce volatility and increase device stability, while at the same time preserving the high device efficiency.

In the majority of previous investigations, the iodide/triiodide couple has been used as a redox mediator, despite the undesirable properties of corrosiveness, volatility and coloration.²² Metal corrosion is particularly problematic since it limits the construction of DSCs on metal substrates and the use of metal charge collection grids. In addition, there is a large difference

between the redox potentials of I[−]/I₃[−] (0.35–0.40 V vs. NHE) and the sensitizer (1.0–1.1 V vs. NHE for N719) corresponding to a potential difference of *ca.* 0.65 V (ΔG^0 63 kJ mol^{−1})—free energy that is dissipated as heat.^{6,22,23}

Attempts to replace the I[−]/I₃[−] couple have included the utilization of redox couples based on TEMPO and its derivatives, thiolates, pseudohalogens, bromide/tribromide, and various transition cobalt, copper and nickel complexes.^{5,23–38} We recently applied ferrocene as an efficient redox mediator.³⁹ In addition to these liquid electrolytes, solid state electrolytes have been developed, with spiro-OMeTAD based DSCs exceeding an efficiency of 6% and copper iodide reaching 4.5%.^{40–44} Progress in electrolyte development has been summarized in recent reviews.^{7,40,45,46} Few of these alternate redox couples have matched the high performance of I[−]/I₃[−]. The new record efficiency for DSCs based on a cobalt(II/III) electrolyte points to the possibility of improving energy conversion efficiencies further by tuning the redox potential of the redox couple.⁵ Little information is available in the current literature on the relationship between the potential of the redox mediators and device efficiency. Although recent reports have shown that optimized difference between the redox level of the electrolyte and dye can lead to improved efficiencies, the limitations require further exploration.^{5,39}

The maximum open circuit voltage (V_{OC}) of the DSC is limited to the difference between the redox potential of the redox mediator and the quasi-Fermi level of electrons in the semiconductor, typically TiO₂. In principle, device efficiencies can be improved by choosing a redox couple with a potential closer to that of the dye, but sufficient driving force needs to be provided to ensure efficient dye regeneration by the redox mediator. In a homogeneous kinetically controlled reaction, a two order of magnitude increase in rate constant can correspond to a 99% increase in reaction yield. If the rate constant for dye regeneration (k_{reg}) is comparable to or smaller than the rate constant for recombination between the injected electron (e[−][TiO₂]) and the dye cation (k_{rec2}), the latter becomes a significant loss mechanism. In the past, attempts to determine the minimum driving force were, by necessity, based on varying the redox potential of the sensitizer (*i.e.*, by using a range of dyes), due to the unavailability of alternatives to I[−]/I₃[−] at that time.^{47,48} As a consequence, the expected voltage output from the devices was similar but, in addition, making significant changes to the sensitizer, including exchanging the metal centre or using organic dyes, could affect the electron transfer kinetics. Oskam *et al.* addressed this issue by investigating the N3 sensitizer in conjunction with three halide and pseudohalide based redox couples.²⁸ It was found that SeCN[−]/SeCN₃[−] and SCN[−]/SCN₃[−] were unable to effectively regenerate the dye whereas, I[−]/I₃[−], a couple with a lower redox potential, was very efficient. Feldt *et al.* studied a series of cobalt(II/III) phenanthroline and bipyridine complexes with varying redox potentials and found that a driving force of 38 kJ mol^{−1} (ΔE 0.39 V) was sufficient to achieve fast dye regeneration.⁴⁹

We recently reported the application of the ferrocene/ferrocenium redox couple in DSCs.³⁹ High efficiencies ($\eta = 7.5\%$) were achieved by excluding oxygen^{39,50,51} during device construction. Furthermore, the use of thin semiconductor films in combination with a strongly absorbing organic dye and chenodeoxycholic

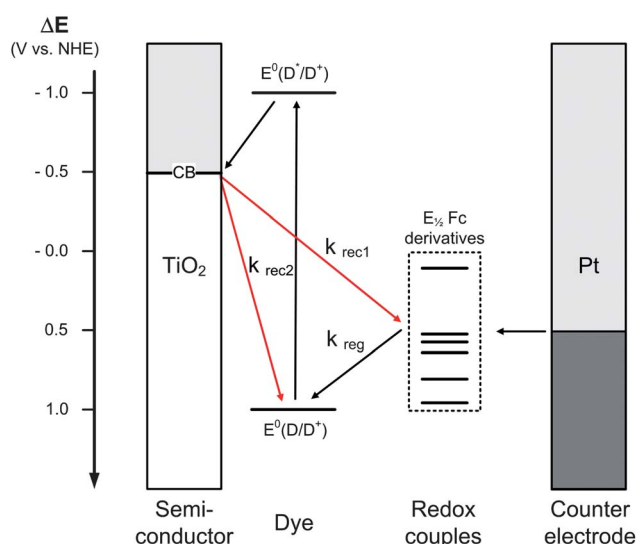


Fig. 1 Energy diagram of the dye-sensitized solar cell with the potentials of the dye, the TiO₂ conduction band and the redox potentials of the investigated ferrocene derivatives. The dye absorbs light, injects an electron into the TiO₂ and is regenerated by the redox shuttle (k_{reg}). Recombination between the injected electron and the oxidized ferrocene species (k_{rec1}) or the oxidized dye (k_{rec2}) may lead to recombination losses.

acid as electrolyte additive reduced recombination losses.³⁹ This $\text{Fc}^{0/+}$ based DSC easily surpassed the efficiency of previous published $\text{Fc}^{0/+}$ DSCs (0.4%)^{52–54} and exhibited higher efficiency than equivalent devices based on I_3^-/I^- . This important result has paved the way for the utilization of a variety of commercial and custom synthesized ferrocene derivatives in DSCs. Redox potentials ranging from 0.1 V to 2 V (vs. NHE) are accessible through alkylation or halogenation of the cyclopentadienyl ring.^{55,56} An examination of the dependence of cell efficiency on the driving force for dye regeneration is reported herein. We compare the efficiency of DSCs prepared using $\text{Fc}^{0/+}$ as a redox mediator with those prepared using $\text{Br}_2\text{Fc}^{0/+}$, $\text{BrFc}^{0/+}$, $\text{EtFc}^{0/+}$, $\text{Et}_2\text{Fc}^{0/+}$ and $\text{Me}_{10}\text{Fc}^{0/+}$. The redox potentials of these derivatives cover a wide range (0.09–0.94 V vs. NHE). The rates of electron transfer processes associated with dye regeneration and charge recombination have been investigated, by the means of transient absorption spectroscopy (TAS) and intensity modulated photovoltage spectroscopy (IMVS), to examine their dependence on the redox potential of the mediator.

Experimental

Materials and reagents

Ferrocene (Fc), tetrabutylammonium hexafluorophosphate (Bu_4NPF_6), lithium bis(trifluoromethanesulfonyl)imide (LiTFSI), solvents and general reagents were purchased from Sigma Aldrich. The ferrocene derivatives (dibromoferrocene (Br_2Fc), bromoferrocene (BrFc), ethylferrocene (EtFc), diethylferrocene (Et_2Fc) and decamethylferrocene (Me_{10}Fc)) and hexachloroplatinic acid were purchased from STREM, silver nitrate from Merck and chenodeoxycholic acid from Acros. The titania pastes were provided by JGC Catalysts and Chemicals Ltd. The organic dye, Carbz-PAHTDIT (Fig. 2), was prepared as described in the literature.³⁹

Synthesis

Silver(I) bis(trifluoromethanesulfonyl)imide–acetonitrile adduct ($\text{AgTFSI} \cdot 2.7\text{CH}_3\text{CN}$). This compound was synthesized by exchanging the lithium ion in commercial LiTFSI with Ag^+ . Both, lithium bis(trifluoromethanesulfonyl)imide (4.30 g, 15 mmol) and silver nitrate (2.54 g, 15 mmol) were dissolved in a 4 : 1 (v/v) mixture of chloroform and acetonitrile (25 mL). The solutions were combined and the mixture was stirred for 2 hours whilst minimizing exposure to light. The resulting suspension

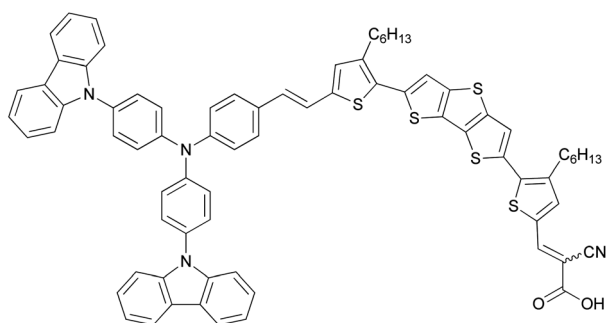


Fig. 2 Structure of the sensitizer Carbz-PAHTDIT.

was filtered under vacuum to remove the precipitated lithium nitrate. After removing the solvent on a rotary evaporator, the product was dissolved in 20 mL of chloroform and the mixture filtered to remove last traces of lithium nitrate. The solvent was again removed to obtain a white crystalline product, which was dried *in vacuo* at 80 °C for 4 hours. $\text{AgTFSI} \cdot 2.7\text{CH}_3\text{CN}$ melts at slightly elevated temperatures and exists as a transparent amber liquid during the drying process. This compound is very hygroscopic and was stored in a nitrogen glovebox. Gravimetric silver analysis by precipitation as AgCl indicated a silver content of 21.6% corresponding to a $\text{Ag}-\text{CH}_3\text{CN}$ ratio of 2.7. Yield of $\text{AgTFSI} \cdot 2.7\text{CH}_3\text{CN}$ (6.25 g, 83%). ^1H NMR (CDCl_3) δ : 2.254 (12H, s, CNCH_3); ^{13}C NMR (CDCl_3) δ : 2.4 (s, RCH_3), 119.2 (s, RCN); 119.8 (q, RCF_3 , $J = 4.27$).

Ferrocenium salts. Samples of each ferrocene derivative (250 mg) and an equimolar amount of $\text{AgTFSI} \cdot \text{CH}_3\text{CN}$ were dissolved in 3 mL dichloromethane under inert atmosphere. The immediate appearance of the characteristic dark blue color of the ferrocenium ion was observed. The mixture was continuously stirred for 1 hour in the dark to ensure completion of the reaction. The precipitated elemental silver was collected by gravity filtration. Removal of the solvent afforded the ferrocenium salts as black-blue solids in the cases of Br_2FcTFSI , BrFcTFSI , FcTFSI and $\text{Me}_{10}\text{FcTFSI}$ and as an ionic liquid for EtFcTFSI and Et_2FcTFSI . All compounds, except for Br_2FcTFSI , were stable when stored under inert atmosphere. The stable ferrocenium TFSI salts were characterized by elemental analysis (SI-T1†) and used without further purification; Br_2FcTFSI was found to decompose slowly over a period of days and hence was used directly after synthesis. Typical yields were above 95%.

Cyclic voltammetry

Cyclic voltammetry was carried out in a nitrogen glovebox with a Biologic VSP potentiostat using a three electrode system comprising a 3 mm diameter Pt disc working electrode, a Ag/AgNO_3 (10 mM) reference electrode and a polished platinum wire as a counter-electrode. Experiments were carried out on 3 mM solutions of each ferrocene compound dissolved in either anhydrous acetonitrile (ACN) or benzonitrile (BZN) containing 0.1 M Bu_4NPF_6 as a supporting electrolyte. The cyclic voltammogram of the dye was recorded adsorbed on a 7×6 mm nanoporous ITO electrode with a film thickness of 1 μm . The reference electrode was calibrated against the redox potential of ferrocene since the electrochemistry of this compound on a Pt electrode is well established ($E_{1/2}\text{Fc} = 0.63$ V vs. NHE in ACN and 0.62 V vs. NHE in BZN).^{56,57}

Electrolyte preparation

Due to the instability of $\text{BrFc}^{0/+}$ and $\text{Br}_2\text{Fc}^{0/+}$ in the presence of 4-tertiarybutylpyridine (*t*BP), an electrolyte formulation free of this additive was developed which could be employed for all ferrocene redox mediators. The electrolytes consisted of the ferrocene derivative (100 mM), oxidized (ferrocenium) derivative (12.5 mM) and chenodeoxycholic acid (10 mM) dissolved in acetonitrile with the exception of $\text{Me}_{10}\text{Fc}^{0/+}$, which is poorly soluble in acetonitrile but sufficiently soluble in benzonitrile.

Cell fabrication

DSC devices were fabricated by established procedures.³⁹ The titanium dioxide films (4×4 mm) used for device construction comprised a $2.3 \mu\text{m}$ thick transparent layer (18 nm particles) and a $6 \mu\text{m}$ scattering layer (400 nm particles) on fluorine-doped tin oxide (FTO) glass and were prepared by screen-printing. Transparent titania films (7×6 mm) for transient absorption spectroscopy were prepared by depositing $0.9 \mu\text{m}$ thick layers of 18 nm titania particles. After initial sintering at 500°C , a TiCl_4 treatment was routinely applied to all films.⁵⁸ Films were sintered at 500°C prior to use in cell fabrication and, while still warm (60°C), were immersed in a 0.2 mM solution of the Carbaz-PAHTDTT dye in a mixture of 75 : 25 (v/v) chloroform and ethanol containing 20 mM chenodeoxycholic acid. After 10 hours, the films were removed from the dye solution, rinsed by immersion in acetonitrile for 5 minutes and dried in a stream of nitrogen. The counter-electrodes were prepared by coating FTO glass slides with a 10 mM ethanol solution of hexachloroplatinic acid and sintering for 15 min at 450°C . The devices were assembled by sandwiching a $25 \mu\text{m}$ thick Surlyn gasket between the photoanodes and platinized counter-electrodes, and then applying heat and pressure to form an airtight seal. As described previously,³⁹ the exclusion of oxygen was important during the vacuum backfilling process in which the electrolyte is introduced into the device and the final back port sealing process using Surlyn coated aluminium foil. These steps were carried out in a nitrogen glovebox (MBraun).

Cell testing

JV characterization. A Keithley 2400 source meter was used to record current density–voltage curves of the DSCs under dark and illuminated conditions. Simulated sunlight was provided by an Oriel sun simulator (1000 W Xe lamp), filtered to provide simulated solar irradiation ($\text{AM}1.5$, 1000 W m^{-2}). A calibrated silicon photodiode (Pecell Technologies) was used to calibrate the output of the light source. The photodiode was fitted with a KG3 filter to minimize the optical mismatch between the calibration diode and DSC. Light intensities of less than one sun were achieved by placing mesh filters in the light path.

Incident photon to electron conversion efficiency (IPCE). The IPCE was measured under short circuit conditions and monochromatic light irradiation. The light was provided by a combination of a Xe lamp (Oriel 150 W) and a monochromator (Cornerstone 260). A calibrated silicon photodiode (Pecell Technologies) was used to quantify the monochromatic photon flux. To account for the shape mismatch between the spherical light beam and the square shaped TiO_2 film, the illumination spot was adjusted to be slightly smaller than the active TiO_2 area. A Keithley 2400 source meter was used to measure the photo-currents.

Transient absorption spectroscopy (TAS). TAS was performed on custom-built instrumentation. A Nd:YAG Q-switched laser (Spectra-Physics INDI 40-10) was used as a pump and a Xe lamp (Edinburg Instruments) in combination with band pass optical filters as a probe beam. DSCs, constructed with and without the redox mediator in the electrolyte, were photo-excited by

nanosecond pulses from the pump laser (532 nm, 6 ns pulses, typical pulse intensity was $3 \mu\text{J cm}^{-2} \text{ pulse}^{-1}$, 10 Hz repetition rate). Changes in transmission were monitored using a combination of a monochromator, fast photo-receivers (Femto) and an oscilloscope (Tektronix) with a total bandwidth of around 100 MHz. Kinetic traces were averaged 1536 times and analyzed using a custom made fitting routine (Labview).

Intensity modulated photo-voltage spectroscopy (IMVS). IMVS was carried out on full devices using a combination of blue and white light LEDs. The blue LED was driven by a purpose built LED driver providing an adjustable DC photon flux. The light intensity of the blue LED was modulated to a depth of 2% by the inbuilt function generator of a Stanford lock-in-amplifier (SR810) providing sine wave modulation between 0.1 Hz and 30 KHz. A white light diode array driven by a commercial DC power source was used to provide additional light intensity to achieve an overall light intensity equivalent to one sun. A filter wheel equipped with a set of neutral density filters was used to adjust the light intensity. All experiments were performed in an earthed Faraday dark-box to eliminate electrical noise at low light intensities. The photo-voltages were measured using a purpose built battery powered high impedance voltage follower (input impedance $10^{12} \Omega$). The phase and amplitude of the resultant AC photo-voltage were captured with a lock-in amplifier (SR810) under computer control (Labview). The measured data were analyzed using a customized fitting program (Labview).

Charge extraction. As for the IMVS measurements, light was supplied by an array of white LEDs combined with a neutral density filter wheel. The DSC was illuminated with unmodulated white light for 10 seconds to reach equilibrium between charge injection and recombination under open circuit conditions. At this point, purpose built computer controlled mercury wetted relay switches simultaneously turned off the light and switched the device to short circuit. The extracted charge was then measured as a voltage across a 50Ω resistor utilizing a NI-6251 data logger.

Results and discussion

Synthesis

A convenient synthesis of the ferrocenium derivatives was developed which was compatible with requirements for their use in DSC electrolytes. Silver(i) salts were found to be suitable oxidants for ferrocene derivatives, offering easy access to the ferrocenium salt with the desired counter-ion.⁵⁹ Reaction of $\text{AgTFSI} \cdot 2.7\text{CH}_3\text{CN}$ with the selected ferrocene derivatives under inert atmosphere (nitrogen glovebox) yielded the ferrocenium TFSI salt and metallic silver. The latter was removed by filtration leaving a solution which could be worked-up to yield the desired salt, in typical yields of >95%. Alternate oxidants, such as the commonly used NOBF_4 or cerium ammonium nitrate, were found to lead to unwanted side reactions and impure final products.

Cyclic voltammetry

Electrochemical studies have previously been conducted on many of the selected ferrocene derivatives.^{56,57,60,61} Nevertheless,

to facilitate comparisons cyclic voltammograms were measured in the solvents used for the DSC electrolytes, acetonitrile and benzonitrile. The electrochemical measurements show that each ferrocene derivative undergoes a reversible one-electron redox process in acetonitrile (Fig. 3). A detailed summary of the parameters derived from CV measurements in acetonitrile and benzonitrile is provided in the ESI† (SI-T2 and SI-T3†). The ratios of peak currents (oxidation/reduction) are close to unity for all compounds and in both solvents indicating a reversible electrochemical process.

Changing the solvent had only minor effects on the redox potential. The diffusion coefficients, determined by measuring cyclic voltammograms at various scan rates and applying the Randles–Sevcik equation,⁶² vary only slightly between the redox couples and are approximately one order of magnitude lower in benzonitrile than in acetonitrile (see Tables SI-T2 and SI-T3†). The diffusion coefficient of ferrocene measured in acetonitrile ($1.9 \times 10^{-5} \text{ cm}^2 \text{ s}^{-1}$) is in good agreement with literature values ($1.6\text{--}2.6 \times 10^{-5} \text{ cm}^2 \text{ s}^{-1}$).⁶³ The introduction of simple alkyl and halogen functional groups has a significant influence on the redox potential of the particular ferrocene derivative, *viz.*, ferrocene compounds studied here span a potential window of $>0.8 \text{ V}$ (see Fig. 3 and Tables SI-T2 and SI-T3†).^{55,56}

The electrochemistry of the dye adsorbed on nano-ITO was more complex, revealing the presence of two redox processes in close proximity, the lower of these being centered at 0.99 V (*vs.* NHE). Overall, the redox potential difference (ΔE) between the dye and the mediator ranges from as low as 0.05 V (Br_2Fc) to 0.90 V (Me_{10}Fc) corresponding to thermodynamic driving forces of 5 to 87 kJ mol^{-1} for electron transfer from the ferrocene to the oxidized dye.

Device performance

Two modifications to our previously published electrolyte³⁹ were made to achieve a meaningful comparison DSC performance for

the six redox couples. Due to the instability of $\text{BrFc}^{0/+}$ and $\text{Br}_2\text{Fc}^{0/+}$ in the presence of 4-tertiarybutylpyridine (*t*BP), an electrolyte free of this additive was developed. *t*BP is commonly added to the electrolytes to adjust the conduction band potential and to increase electron lifetime.⁶⁴ Indeed, the addition of this agent to $\text{Fc}^{0/+}$ electrolytes contributed to the achievement of a 7.5% efficiency.³⁹ Due to instrument limitations, the concentration of the oxidized species was reduced from 50 mM to 12.5 mM , in order to measure the rates of charge recombination. Nevertheless, efficiencies of up to $5.2 \pm 0.2\%$ were achieved for unsubstituted ferrocene at AM $1.5 \text{ } 100 \text{ mW cm}^{-2}$ simulated sunlight in this study (SI-T4†). The main differences between these new results and our previously data³⁹ are the lower open circuit potentials (0.74 V *vs.* 0.84 V) due to the absence of *t*BP and a lower fill factor (0.57 *vs.* 0.73) caused by lower concentrations of the oxidized redox mediator. DSCs mediated by $\text{Me}_{10}\text{Fc}^{0/+}$ showed a sublinear dependence of short circuit current on light intensity due to the use of the more viscous benzonitrile as an electrolyte solvent, leading to diffusion limitations. The results obtained at 10 mW cm^{-2} were found to be suitable for comparison of the six ferrocene derivatives and will be discussed herein. Full J – V characterization is available in the ESI (SI-T4†).

The dependence of the V_{OC} on the driving force for dye regeneration is shown in Fig. 4a. The measured V_{OC} values should mirror the increase in redox potential as this leads to a larger difference in the potentials of the quasi-Fermi level of the electrons in the TiO_2 and redox mediator. Indeed, this is the case for electrolytes starting from $\text{Me}_{10}\text{Fc}^{0/+}$ until $\text{Fc}^{0/+}$. For DSCs mediated by $\text{Et}_2\text{Fc}^{0/+}$, $\text{EtFc}^{0/+}$ and $\text{Fc}^{0/+}$ the difference in V_{OC} approximately equals the difference in $E_{1/2}$ values and, thus the V_{OC} follows the expected trend. Although $\text{Me}_{10}\text{Fc}^{0/+}$ mediated devices show a lower V_{OC} than Et_2Fc DSCs, the difference falls short of the expected 0.42 V . This result will be discussed in conjunction with charge extraction measurements. In the case of $\text{BrFc}^{0/+}$ and $\text{Br}_2\text{Fc}^{0/+}$, the V_{OC} values were lower than expected from the increase in redox potential.

The short circuit current (Fig. 4b) is identical for electrolytes with driving forces larger than 35 kJ mol^{-1} ($\Delta E 0.36 \text{ V}$), whereas $\text{BrFc}^{0/+}$ and $\text{Br}_2\text{Fc}^{0/+}$ show reduced photo-current densities. Analysis of the IPCE spectra for devices constructed with each ferrocene derivative reveals that the IPCE_{max} values correlate well with the trend of the short circuit current.

Determination of k_{rec2} and k_{reg}

Transient absorption spectroscopy (TAS) is frequently used to study dye regeneration kinetics in DSCs.^{42,65} In this experiment, a dye-sensitized TiO_2 film is excited with a laser pulse whereupon the excited dye injects an electron into the TiO_2 and is oxidized forming a dye cation (dye^+) with an absorption spectrum different to its ground state. The changes in optical transmission of the sample following the laser pulse are monitored at selected wavelengths by means of a probe light beam and a photo-detector. The dye^+ lifetime and rate of recombination between injected electrons and dye^+ can be determined from measurements of the transient absorption of dye-sensitized films in contact with an inert electrolyte (not containing a redox couple). Experiments in the presence of a redox couple allow the rate of dye regeneration to be established. The observed transient absorption signal is

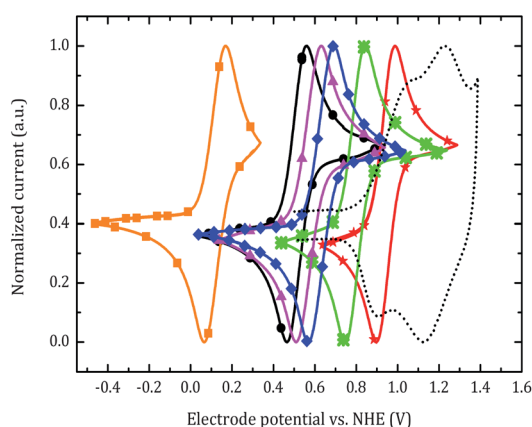


Fig. 3 Normalized cyclic voltammograms of Br_2Fc (red stars), BrFc (green snowflakes), ferrocene (blue diamonds), EtFc (pink triangles), Et_2Fc (black circles) and Me_{10}Fc (orange squares) measured on 3 mM solutions of each compound dissolved in acetonitrile containing 0.1 M Bu_4NPF_6 as a supporting electrolyte. The CV of the dye (dotted black line) was recorded adsorbed onto a nanoporous ITO electrode. The CVs were measured *vs.* Ag/AgNO_3 at a scan rate of 20 mV s^{-1} and converted to the NHE scale using $E_{1/2}(\text{Fc}) = 0.63 \text{ V vs. NHE}$.⁵⁷

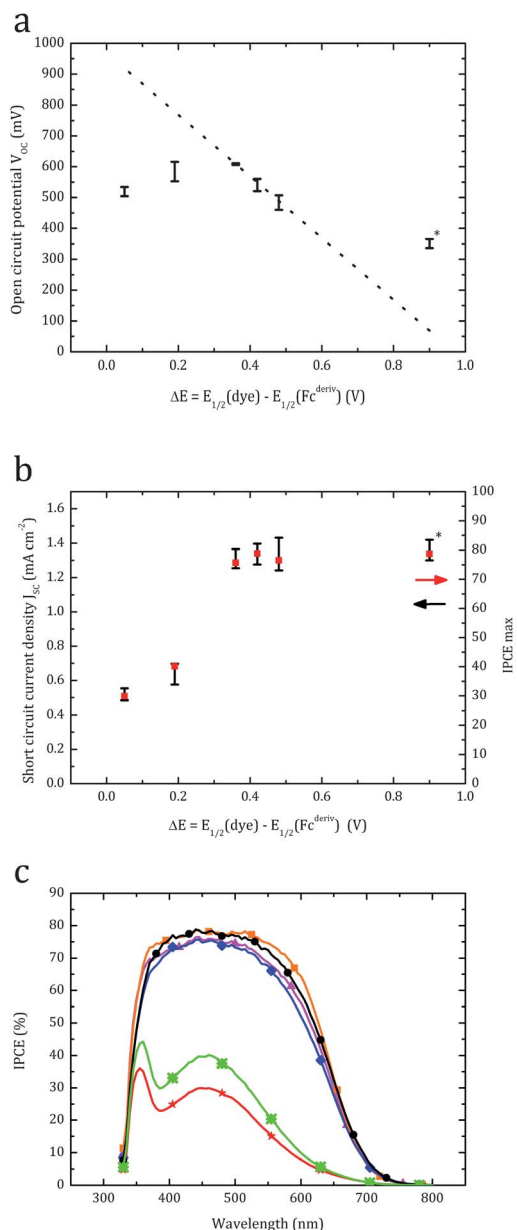


Fig. 4 (a) Open circuit potential (V_{OC}) vs. potential difference ΔE measured at AM1.5 100 mW cm⁻². The dotted line shows the extrapolated dependence calculated by subtracting the difference in redox potential from the V_{OC} measured for unsubstituted ferrocene ($V_{OC}(\Delta E) = V_{OC}(\text{Fc}) - (\Delta E - \Delta E(\text{Fc}))$). (b) Short circuit current density J_{SC} (black) and incident photon to electron conversion efficiency IPCE (red) vs. driving force for dye regeneration (ΔE). J_{SC} and V_{OC} data were averaged from 3 devices. Me₁₀Fc mediated devices (*) utilized benzonitrile as a solvent, other devices acetonitrile. (c) IPCE spectra of devices mediated by Br₂Fc (red stars), BrFc (green snowflakes), ferrocene (blue diamonds), EtFc (pink triangles), Et₂Fc (black circles) and Me₁₀Fc (orange squares).

proportional to the difference in extinction coefficients of $\epsilon(\text{dye}^+)$ and the sum of $(\epsilon(\text{dye}^0) + \epsilon(e^-_{\text{TiO}_2}))$.

Fig. 5 shows the transient absorption spectrum of a TiO₂ film sensitized with Carbz-PAHTDIT in contact with an inert electrolyte (acetonitrile containing 10 mM chenodeoxycholic acid) measured 300 ns after laser excitation. The time $t = 300$ ns was

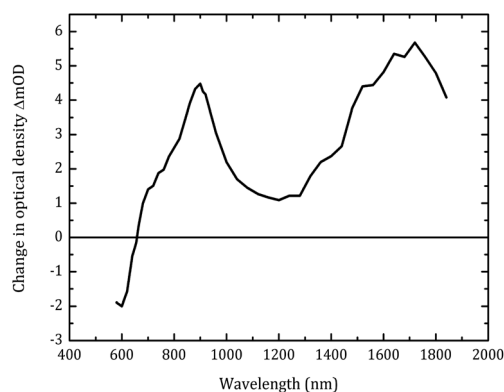


Fig. 5 Transient absorption spectrum of a TiO₂ film sensitized with Carbz-PAHTDIT measured 300 ns after laser excitation in the absence of a redox couple. The electrolyte contained 10 mM chenodeoxycholic acid in acetonitrile. Laser excitation wavelength: 532 nm, pulse energy: 3 $\mu\text{J cm}^{-2}$, repetition rate: 10 Hz.

chosen since the initial signal noise has disappeared and absorbance magnitude is still at its maximum (see Fig. 6a). It shows two characteristic positive transient absorption peaks at 900 nm and 1700 nm, in accordance to spectral features previously observed for oxidized carbazole containing dyes.⁶⁶ As previously observed,⁶⁷ a negative change in optical density can be observed below 630 nm, which is attributed to dye ground state bleaching and a Stark shift. In the following experiments, an observation wavelength of 900 nm was chosen to study dye regeneration.

To determine the rate of dye regeneration, the reduced form of the ferrocene couples was added to the electrolyte. This accelerated the dye⁺ decay as it could also return to the ground state by reaction with the ferrocenes. Initial experiments showed that high concentrations (100 mM) of the unsubstituted ferrocene in the DSC electrolytes result in regeneration rates that were too fast to measure with our experimental setup. Testing of a series of different concentrations (Fig. SI-F1 in the ESI[†]) showed that a 5 mM solution was most suitable to resolve the regeneration between dye⁺ and Fc, EtFc, Et₂Fc and Me₁₀Fc. The decay of the dye⁺ signal in the absence and presence of the ferrocene derivatives in the electrolyte solution in Fig. 6 clearly indicates that dye regeneration occurred within 10 μs for most of the studied ferrocene derivatives. The observed absorption decay profiles followed the order Me₁₀Fc \approx Et₂Fc \approx EtFc \approx Fc > BrFc > Br₂Fc. The brominated compounds were slow to convert dye⁺ into dye⁰ whereas the other derivatives regenerate the dye rapidly in comparison to the dye⁺ lifetime.

Increasing the concentration of BrFc and Br₂Fc from 5 mM to 100 mM (Fig. 6c) accelerates dye regeneration for BrFc, while Br₂Fc showed little change. These experiments imply that under the experimental conditions (open circuit) a driving force >18 kJ mol⁻¹ (ΔE 0.19 V) is necessary to achieve fast dye regeneration. On switching solvents from acetonitrile to benzonitrile, the dye⁺ lifetime in the absence of a redox mediator is significantly shorter. Moreover, the rate of dye regeneration is faster in acetonitrile than in benzonitrile.

The kinetics of dye regeneration are typically modeled with a stretched exponential decay.⁶⁵ The dye regeneration rate constant, k_{reg} , can be calculated using eqn (1)–(5), where τ_{ww} is

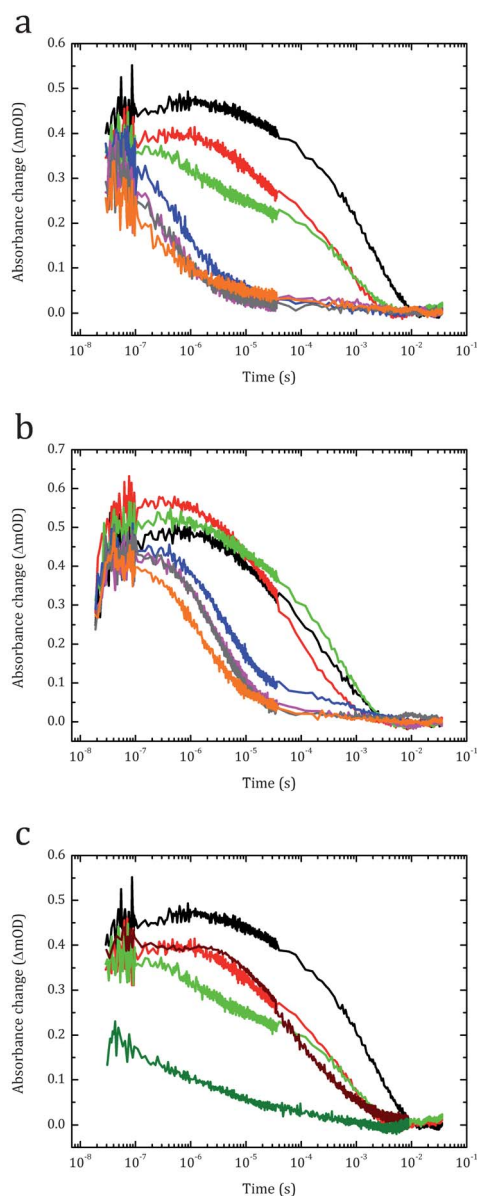


Fig. 6 Transient absorption decay at 900 nm observed for dye-sensitized TiO₂ films in the absence (black), and in the presence of 5 mM of Br₂Fc (red), BrFc (green), Fc (blue), EtFc (pink), Et₂Fc (grey), Me₁₀Fc (orange) in (a) acetonitrile and (b) benzonitrile, containing 10 mM chenodeoxycholic acid. Measurements with higher BrFc and Br₂Fc concentration are shown in (c). Inert electrolyte (black) 5 mM Br₂Fc (red), 100 mM Br₂Fc (maroon), 5 mM BrFc (green), and 100 mM BrFc (dark green) measured in acetonitrile containing 10 mM chenodeoxycholic acid. Laser excitation wavelength: 532 nm, pulse energy: 3 μJ cm⁻², repetition rate: 10 Hz.

the characteristic stretched lifetime, β is the stretch parameter, and Γ is the gamma function. $\Delta OD_{(t)}$ is the measured change in optical density, and $\Delta OD_{(t=0)}$ is the initial change in optical density, directly after laser induced formation of dye⁺. τ_{obs} is the weighted average lifetime of the stretched exponential and k_{obs} is the observed rate constant for dye regeneration. The recombination between injected electrons and dye⁺ (k_{rec2}) is measured on a device containing an inert electrolyte without the redox couple. The gamma function (eqn (5)) is an integral with the boundaries

of 0 and infinity while u is the variable of integration. The concentration of the ferrocene derivative is [Fc^{deriv}]:

$$\Delta OD_{(t)} = \Delta OD_{(t=0)} e^{-(t/\tau_{\text{ww}})^\beta} \quad (1)$$

$$\tau_{\text{obs}} = \frac{\tau_{\text{ww}}}{\beta} \Gamma\left(\frac{1}{\beta}\right) \quad (2)$$

$$k_{\text{obs}} = \frac{1}{\tau_{\text{obs}}} \quad (3)$$

$$k_{\text{reg}} = \frac{k_{\text{obs}} - k_{\text{rec2}}}{[\text{Fc}^{\text{deriv}}]} \quad (4)$$

$$\Gamma\left(\frac{1}{\beta}\right) = \int_0^\infty u^{\frac{1}{\beta}-1} e^{-u} du \quad (5)$$

The dependence of k_{obs} on the difference in the redox potentials of the dye and ferrocene derivative is summarized in Fig. 7. The results and fitted parameters can be found in Table SI-T5 of the ESI†. The stretched exponential decay was found to give good fits to the measured data.

The k_{obs} determined in the absence of the ferrocene derivative in the electrolyte ($k_{\text{obs}} = k_{\text{rec2}}$) were $k_{\text{rec2}} = 320 (\pm 10) \text{ s}^{-1}$ in acetonitrile and $k_{\text{rec2}} = 1250 (\pm 50) \text{ s}^{-1}$ in benzonitrile. The fact that these k_{rec2} values are very similar to the k_{obs} values measured for Br₂Fc and BrFc indicates that these compounds react relatively slowly with the oxidized dye and, as a consequence, significant recombination losses arise from the reaction of dye⁺ and the injected electrons. Fast dye regeneration rates were observed for the other four ferrocenes with a driving force $\geq 35 \text{ kJ mol}^{-1}$ ($\Delta E 0.36 \text{ V}$). In these cases, the fact that dye regeneration by the redox mediator (k_{reg}) is several orders of magnitude faster than k_{rec2} means that recombination between dye⁺ and the injected electrons will be suppressed. For the compounds facilitating sufficiently fast dye regeneration, the rate constants k_{reg} were calculated according to eqn (4) (see Table 1). Following a literature precedent,⁴⁹ a regeneration yield Φ under electrolyte conditions (ferrocene derivative concentration = 100 mM) was

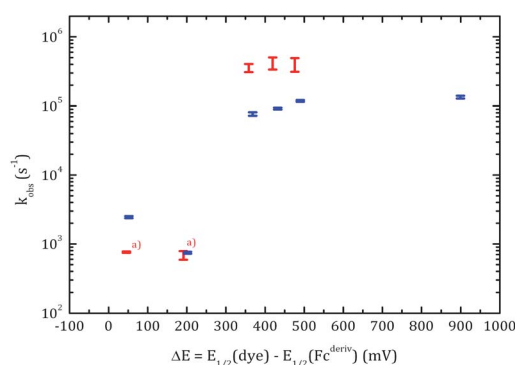


Fig. 7 Dependence of the observed dye regeneration rate on the potential difference between the oxidized dye and the redox potential of the mediator in acetonitrile (red) and benzonitrile (blue) containing 10 mM chenodeoxycholic acid for a 5 mM concentration of the ferrocene derivatives. (a) indicates a concentration of 100 mM. The error bars indicate the uncertainty of the fit in each value.

estimated from TAS data (measured at open circuit) using eqn (6):

$$\Phi = \left(1 - \frac{k_{\text{rec2}}}{k_{\text{reg}}[\text{Fc}^{\text{deriv}}]0.1 \text{ M} + k_{\text{rec2}}} \right) \times 100\% \quad (6)$$

The rate constants for dye regeneration are very similar for Fc, EtFc, Et₂Fc and Me₁₀Fc. In sharp contrast, k_{reg} in the case of BrFc is 20 000 times smaller than for Fc. This indicates that for driving forces $\geq 35 \text{ kJ mol}^{-1}$ (ΔE 0.36 V) dye regeneration is not limited by the driving force but is instead diffusion limited. On average, the k_{reg} values measured in acetonitrile were about 4 times larger when compared to benzonitrile. This is likely to be a consequence of the 3.4 fold higher viscosity of benzonitrile (at 25 °C) leading to decreased diffusion rates.⁶⁸ Regeneration yields were estimated to be above 99.9% in the cases of Fc, EtFc, Et₂Fc and Me₁₀Fc and 53% for BrFc. Several values can be found in the literature for the rate constant for dye regeneration by iodide. Anderson *et al.* reviewed the literature and reported a k_{reg} value of $7.8 \times 10^5 \text{ M}^{-1} \text{ s}^{-1}$ for the N719 sensitizer measured in 3-methoxypropionitrile.⁶⁵ In comparison, the k_{reg} value for ferrocene is 20 (benzonitrile) to 90 (acetonitrile) times larger and the regeneration reaction becomes diffusion controlled for driving forces of $\geq 35 \text{ kJ mol}^{-1}$. The reaction of ferrocene with the oxidized dye is a one-electron process that involves little molecular reorganization during electron transfer. For dye regeneration by iodide, on the other hand, larger driving forces are required in order to overcome the mechanistic complexity of this two electron redox process.²² For example, Clifford *et al.* have found that Ru^{II}(dcbpy)₂Cl₂ (dcbpy = 2,2'-bipyridine-4,4'-dicarboxylic acid) is not regenerated by iodide (44 kJ mol⁻¹; ΔE 0.46 V) but that Ru^{II}(dcbpy)₂DTC (DTC = diethyldithiocarbamate) is regenerated efficiently (68 kJ mol⁻¹; ΔE 0.70 V).⁴⁷ Oskam *et al.* reached a similar conclusion in studies of N3 and a series of pseudohalogenes.²⁸ The dye was not regenerated by SeCN⁻ even though the driving force exceeded 43 kJ mol⁻¹ (ΔE 0.45 V). The two electron tetramethylformaminium disulfide/tetramethylthiourea redox shuttle could not effectively regenerate Z907 (35 kJ mol⁻¹; ΔE 0.36 V) whereas an organic dye with a higher redox potential (61 kJ mol⁻¹; ΔE 0.63 V) worked efficiently.⁶⁹ The consensus is that single electron redox couples,

such as the ferrocenes investigated herein, provide a lower activation energy pathway and require less driving force to achieve efficient regeneration. In this context, Feldt *et al.* in their investigation of a series of cobalt complexes as redox mediators found that 80% of the photo-generated dye cations were regenerated by a driving force of 38 kJ mol⁻¹ (ΔE 0.39 V).⁴⁹

Electrolyte recombination R_{rec1}

The recombination reaction between the injected electron and the oxidized mediator can be followed by intensity modulated photo-voltage spectroscopy (IMVS). In IMVS, the solar cell is kept under open circuit conditions and is illuminated by a constant light intensity on top of which frequency modulated sine-wave illumination is added. As the electron lifetime varies with electron density in the TiO₂ and thus with light intensity, the perturbation amplitude has to be much smaller than the constant bias illumination, in order to determine the electron lifetime under defined conditions. The modulation was kept <2% of the total light intensity at all times and the overall light intensity was adjusted by neutral density filters. The AC component of the photo-voltage response and the phase shift are measured over a range of frequencies (typically between 0.1 Hz and 30 KHz). The IMVS plot shows the characteristic semicircle (Fig. SI-F2 in the ESI†). The minimum of the semicircle is located at $2\pi^*f_{\text{min}} = 1/\tau_n$, where f_{min} is the frequency associated with the minimum of the semicircle and τ_n is the electron lifetime.^{70,71} Charge extraction measurements⁷² were attempted to determine the electron density but the time needed to extract the charge was found to be longer than the electron lifetime. Hence, during charge extraction an unquantifiable but significant percentage of charge carriers recombine leading to an underestimation of the charge density (Fig. SI-F3 to SI-F7 in the ESI†). Since the open circuit voltage is a function of the difference between the redox potential of the electrolyte and the quasi-Fermi level of the TiO₂, which in turn is dependent on the charge density in the TiO₂, the electron lifetimes can be compared at the same open circuit voltage provided a correction is made for differences in the potential of the redox couples and that no change in electron trap density and distribution has occurred (eqn (7)). The dependence of the experimentally determined electron lifetime on the normalized V_{OC} is shown in Fig. 8:

$$V_{\text{OC}}(\text{normalized}) = V_{\text{OC}} + (E_{1/2}[\text{Fc}] - E_{1/2}[\text{Fc}^{\text{deriv}}]) \quad (7)$$

The dependence of the electron lifetime on the normalized V_{OC} is the same for Fc, EtFc and Et₂Fc, indicating similar recombination rates. This is not the case for the other three redox couples. Firstly, Me₁₀Fc shows a significantly longer electron lifetime at the same normalized V_{OC} . Even though not all charge could be extracted, the charge extraction measurements (Fig. SI-F8 in the ESI†) indicate that a change in the electrolyte solvent from acetonitrile to benzonitrile causes a shift in the conduction band. This also accounts for the higher than expected V_{OC} for the Me₁₀Fc mediated devices. Secondly, the electron lifetimes at given normalized V_{OC} are much shorter for BrFc and Br₂Fc. In fact, electron lifetimes could not be measured for Br₂Fc using our experimental setup.

Table 1 Dye regeneration rate constants (k_{reg}) determined from TAS measurements

	$E_{1/2}$ (V vs. NHE)	ΔE^d (V)	$k_{\text{reg}}/10^6 \text{ M}^{-1} \text{ s}^{-1}$	Φ (%)
<i>Acetonitrile</i>				
BrFc ^b	0.80	0.19	0.0037 (± 0.0009)	53.4
Fc	0.63	0.36	71 (± 10)	>99.9
EtFc	0.57	0.42	84 (± 17)	>99.9
Et ₂ Fc	0.51	0.48	80 (± 18)	>99.9
<i>Benzonitrile</i>				
Fc	0.62	0.37	15.2 (± 0.9)	98.4
EtFc	0.56	0.43	18.2 (± 0.6)	98.6
Et ₂ Fc	0.50	0.49	23.4 (± 0.7)	98.9
Me ₁₀ Fc ^c	0.09	0.90	27 (± 1)	99.1

^a Difference between the redox potential of the dye and the ferrocene derivative. ^b Measured with a concentration of 100 mM. ^c Insufficiently soluble in acetonitrile for measurement.

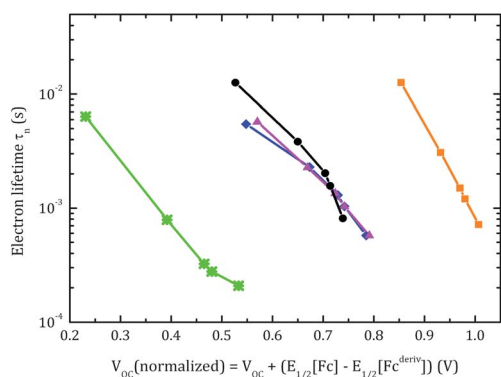


Fig. 8 Electron lifetime vs. normalized V_{OC} , measured on devices containing 100 mM of the reduced species, 12.5 mM of the oxidized species and 10 mM chenodeoxycholic acid in acetonitrile for BrFc (green—snowflakes), Fc (blue—diamonds), EtFc (pink—triangles), Et₂Fc (black—circles) and benzonitrile for Me₁₀Fc (orange—squares).

The variation in the recombination rates with the redox potential of the mediator is not monotonic. Rather than a gradual decrease of the electron lifetime as a function of increasing redox potential of the redox couple, a dramatic change in electron lifetime is observed at a threshold potential difference of 0.36 V between the dye and the redox couple. This potential difference was previously shown to provide sufficient driving force to achieve efficient dye regeneration. Redox couples with higher driving forces for dye regeneration show similar recombination rates.

In a DSC, the injected electron can recombine either with the oxidized species of the redox shuttle (rec1) or with the photo-generated dye⁺ cation (rec2). Fast reaction of dye⁺ with the redox shuttle implies that the concentration of dye⁺ is low, so that no significant reaction is observed between the injected electron and dye⁺. As shown above, this is indeed the case for Fc, EtFc, Et₂Fc and Me₁₀Fc. When dye regeneration by the reduced mediator is slow, the recombination pathway (rec2) becomes possible, which is responsible for the short electron lifetime measured using the BrFc and Br₂Fc couples. Our findings show that the recombination reaction with the oxidized mediator rec1 is either weakly dependent or independent of the redox potential, whereas recombination with dye⁺ (rec2) is redox potential dependent due to an increase in the concentration of dye⁺ in cases where dye regeneration is limited by small driving forces. Published studies complementing measurements of the electron lifetimes with dye regeneration studies support our interpretation of the results. Feldt *et al.*⁴⁹ found efficient dye regeneration and close to identical electron lifetimes for [Co(phen)₃]^{2+/3+} and [Co(Cl-phen)₃]^{2+/3+} redox shuttles whereas slow dye regeneration and a shorter electron lifetime were observed for [Co(NO₂-phen)₃]^{2+/3+}. The interpretation of our results is in keeping with the findings of Oskam *et al.* who reported that N3-sensitized solar cells mediated by SeCN⁻/SeCN₃⁻ and SCN⁻/SCN₃⁻ suffered from insufficient dye regeneration, resulting in accelerated recombination to the oxidized dye.²⁸

Conclusions

A series of ferrocene derivatives covering a redox potential range of 0.09 to 0.94 V vs. NHE were investigated as mediators for dye-sensitized solar cells. Similar solar conversion efficiencies

(4.3–5.2%) and IPCEs were achieved when using ferrocene and two ethyl derivatives, Et₂Fc and EtFc, with the slightly lower efficiencies for the alkylated redox mediators reflecting differences in the redox potentials and concomitant decreases in the open circuit voltage. The halogen ferrocene derivatives, BrFc and Br₂Fc, showed lower energy conversion efficiencies than Et₂Fc, EtFc and Fc despite their more favorable redox potential. Transient absorption measurements revealed that Et₂Fc, EtFc and Fc, which provide driving forces of 35–46 kJ mol⁻¹, promote fast dye regeneration by rapidly reacting with the photo-oxidized dye, whereas this is not the case for BrFc and Br₂Fc in which case the driving forces are ≤18 kJ mol⁻¹. For BrFc and Br₂Fc, the increased concentration of dye⁺ under operational conditions leads to accelerated recombination between the injected electrons and dye⁺ accompanied by photo-current and photo-voltage losses and reduced conversion efficiencies. Furthermore, investigations of the recombination kinetics revealed that, as long as the dye is regenerated efficiently, the electron lifetime is weakly dependent or independent of the redox potential of the mediator.

This study has identified that the ideal driving force for dye regeneration lies between 18 and 35 kJ mol⁻¹ (ΔE 0.19 to 0.36 V). A further study focusing within this tight range of driving forces, utilizing more ferrocene derivatives and a series of related dyes with varying potentials, could more precisely define the minimum driving force required for efficient reaction.

To increase the efficiency of ferrocene based DSCs, we conclude that the ferrocene derivatives should be matched to dyes with appropriate energy levels, such that $\Delta E \approx 0.36$ V. Following this approach, redox couples such as BrFc could be utilised in conjunction with dyes showing a higher D/D⁺ potential leading to increased open circuit voltages. Alternatively, alkylated ferrocene derivatives could be used in conjunction with panchromatic dyes which have lower D/D⁺ potentials, and leading to high short circuit current densities.

Acknowledgements

Financial support from the Australian Research Council through the Australian Centre of Excellence for Electromaterials Science (ACES), and the Discovery, Australian Research Fellowship and LIEF programs, the Commonwealth Scientific and Industrial Research Organization (Australia), the Australian Solar Institute, the Victorian State Government Department of Primary Industry (SERD Program, Victorian Organic Solar Cells Consortium) and Monash University for supporting U.B. with a Monash Research Fellowship are gratefully acknowledged. AJM acknowledges the support from the ARC through Linkages and Discovery Grants and an ARF Fellowship. We also thank Ms Monika Fekete for providing screen printed nanoporous ITO films.

Notes and references

- B. O'Regan and M. Grätzel, *Nature*, 1991, **353**, 737–740.
- C.-Y. Chen, M. Wang, J.-Y. Li, N. Pootrakulchote, L. Alibabaei, C.-h. Ngoc-le, J.-D. Decoppet, J.-H. Tsai, C. Grätzel, C.-G. Wu, S. M. Zakeeruddin and M. Grätzel, *ACS Nano*, 2009, **3**, 3103–3109.
- Q. Yu, Y. Wang, Z. Yi, N. Zu, J. Zhang, M. Zhang and P. Wang, *ACS Nano*, 2010, **4**, 6032–6038.
- J. N. Clifford, E. Martinez-Ferrero, A. Viterisi and E. Palomares, *Chem. Soc. Rev.*, 2011, **40**, 1635–1646.

- 5 A. Yella, H.-W. Lee, H. N. Tsao, C. Yi, A. K. Chandiran, M. K. Nazeeruddin, E. W.-G. Diao, C.-Y. Yeh, S. M. Zakeeruddin and M. Grätzel, *Science*, 2011, **334**, 629–634.
- 6 T. Bessho, E. Yoneda, J.-H. Yum, M. Guglielmi, I. Tavernelli, H. Imai, U. Rothlisberger, M. K. Nazeeruddin and M. Grätzel, *J. Am. Chem. Soc.*, 2009, **131**, 5930–5934.
- 7 A. Hagfeldt, G. Boschloo, L. Sun, L. Kloo and H. Pettersson, *Chem. Rev.*, 2010, **110**, 6595–6663.
- 8 C.-C. Chou, K.-L. Wu, Y. Chi, W.-P. Hu, S. J. Yu, G.-H. Lee, C.-L. Lin and P.-T. Chou, *Angew. Chem., Int. Ed.*, 2011, **50**, 2054–2058.
- 9 P. Pechy, T. Renouard, S. M. Zakeeruddin, R. Humphry-Baker, P. Comte, P. Liska, L. Cevey, E. Costa, V. Shklover, L. Spiccia, G. B. Deacon, C. A. Bignozzi and M. Grätzel, *J. Am. Chem. Soc.*, 2001, **123**, 1613–1624.
- 10 A. Mishra, M. K. R. Fischer and P. Baeuerle, *Angew. Chem., Int. Ed.*, 2009, **48**, 2474–2499.
- 11 K. Hara, M. Kurashige, Y. Dan-oh, C. Kasada, A. Shinpo, S. Suga, K. Sayama and H. Arakawa, *New J. Chem.*, 2003, **27**, 783–785.
- 12 W. M. Campbell, K. W. Jolley, P. Wagner, K. Wagner, P. J. Walsh, K. C. Gordon, L. Schmidt-Mende, M. K. Nazeeruddin, Q. Wang, M. Grätzel and D. L. Officer, *J. Phys. Chem. C*, 2007, **111**, 11760–11762.
- 13 S. Ito, H. Miura, S. Uchida, M. Takata, K. Sumioka, P. Liska, P. Comte, P. Pechy and M. Grätzel, *Chem. Commun.*, 2008, 5194–5196.
- 14 T. Bessho, S. M. Zakeeruddin, C.-Y. Yeh, E. W.-G. Diao and M. Grätzel, *Angew. Chem., Int. Ed.*, 2010, **122**, 6796–6799.
- 15 W. Zeng, Y. Cao, Y. Bai, Y. Wang, Y. Shi, M. Zhang, F. Wang, C. Pan and P. Wang, *Chem. Mater.*, 2010, **22**, 1915–1925.
- 16 B. E. Hardin, E. T. Hoke, P. B. Armstrong, J.-H. Yum, P. Comte, T. Torres, J. M. J. Frechet, M. K. Nazeeruddin, M. Grätzel and M. D. McGehee, *Nat. Photonics*, 2009, **3**, 406–411.
- 17 K. Lee, S. W. Park, M. J. Ko, K. Kim and N.-G. Park, *Nat. Mater.*, 2009, **8**, 665–671.
- 18 S. Ito, S. M. Zakeeruddin, P. Comte, P. Liska, D. Kuang and M. Grätzel, *Nat. Photonics*, 2008, **2**, 693–698.
- 19 Y. Bai, Y. Cao, J. Zhang, M. Wang, R. Li, P. Wang, S. M. Zakeeruddin and M. Grätzel, *Nat. Mater.*, 2008, **7**, 626–630.
- 20 P. Wang, Q. Dai, S. M. Zakeeruddin, M. Forsyth, D. R. MacFarlane and M. Grätzel, *J. Am. Chem. Soc.*, 2004, **126**, 13590–13591.
- 21 P. Wang, S. M. Zakeeruddin, J. E. Moser, M. K. Nazeeruddin, T. Sekiguchi and M. Grätzel, *Nat. Mater.*, 2003, **2**, 402–407.
- 22 G. Boschloo and A. Hagfeldt, *Acc. Chem. Res.*, 2009, **42**, 1819–1826.
- 23 Z. Zhang, P. Chen, T. N. Murakami, S. M. Zakeeruddin and M. Grätzel, *Adv. Funct. Mater.*, 2008, **18**, 341–346.
- 24 F. Kato, N. Hayashi, T. Murakami, C. Okumura, K. Oyaizu and H. Nishide, *Chem. Lett.*, 2010, 464–465.
- 25 M. Wang, N. Chamberland, L. Breaux, J.-E. Moser, R. Humphry-Baker, B. Marsan, S. M. Zakeeruddin and M. Grätzel, *Nat. Chem.*, 2010, **2**, 385–389.
- 26 H. Tian, X. Jiang, Z. Yu, L. Kloo, A. Hagfeldt and L. Sun, *Angew. Chem., Int. Ed.*, 2010, **49**, 7328–7331.
- 27 D. Li, H. Li, Y. Luo, K. Li, Q. Meng, M. Armand and L. Chen, *Adv. Funct. Mater.*, 2010, **20**, 3358–3365.
- 28 G. Oskam, B. V. Bergeron, G. J. Meyer and P. C. Searson, *J. Phys. Chem. B*, 2001, **105**, 6867–6873.
- 29 P. Wang, S. M. Zakeeruddin, J.-E. Moser, R. Humphry-Baker and M. Grätzel, *J. Am. Chem. Soc.*, 2004, **126**, 7164–7165.
- 30 C. Teng, X. Yang, C. Yuan, C. Li, R. Chen, H. Tian, S. Li, A. Hagfeldt and L. Sun, *Org. Lett.*, 2009, **11**, 5542–5545.
- 31 C. Teng, X. Yang, S. Li, M. Cheng, A. Hagfeldt, L.-z. Wu and L. Sun, *Chem.–Eur. J.*, 2010, **16**, 13127–13138.
- 32 H. Nusbaumer, J.-E. Moser, S. M. Zakeeruddin, M. K. Nazeeruddin and M. Grätzel, *J. Phys. Chem. B*, 2001, **105**, 10461–10464.
- 33 S. M. Feldt, E. A. Gibson, E. Gabriellson, L. Sun, G. Boschloo and A. Hagfeldt, *J. Am. Chem. Soc.*, 2010, **132**, 16714–16724.
- 34 D. Zhou, Q. Yu, N. Cai, Y. Bai, Y. Wang and P. Wang, *Energy Environ. Sci.*, 2011, **4**, 2030–2034.
- 35 Y. Bai, Q. Yu, N. Cai, Y. Wang, M. Zhang and P. Wang, *Chem. Commun.*, 2011, **47**, 4376–4378.
- 36 S. Hattori, Y. Wada, S. Yanagida and S. Fukuzumi, *J. Am. Chem. Soc.*, 2005, **127**, 9648–9654.
- 37 T. C. Li, A. M. Spokoyny, C. She, O. K. Farha, C. A. Mirkin, T. J. Marks and J. T. Hupp, *J. Am. Chem. Soc.*, 2010, **132**, 4580–4582.
- 38 A. M. Spokoyny, T. C. Li, O. K. Farha, C. W. Machan, C. She, C. L. Stern, T. J. Marks, J. T. Hupp and C. A. Mirkin, *Angew. Chem., Int. Ed.*, 2010, **49**, 5339–5343.
- 39 T. Daeneke, T.-H. Kwon, A. B. Holmes, N. W. Duffy, U. Bach and L. Spiccia, *Nat. Chem.*, 2011, **3**, 213–217.
- 40 S. Yanagida, Y. Yu and K. Manseki, *Acc. Chem. Res.*, 2009, **42**, 1827–1838.
- 41 U. Bach, D. Lupo, P. Comte, J. E. Moser, F. Weissortel, J. Salbeck, H. Spreitzer and M. Grätzel, *Nature*, 1998, **395**, 583–585.
- 42 A. J. Mozer, D. K. Panda, S. Gambhir, B. Winther-Jensen and G. G. Wallace, *J. Am. Chem. Soc.*, 2010, **132**, 9543–9545.
- 43 N. Cai, S.-J. Moon, L. Cevey-Ha, T. Moehl, R. Humphry-Baker, P. Wang, S. M. Zakeeruddin and M. Grätzel, *Nano Lett.*, 2011, 1452–1456.
- 44 K. Tennakone, *et al.*, *J. Phys. D: Appl. Phys.*, 1998, **31**, 1492–1496.
- 45 T. W. Hamann and J. W. Ondersma, *Energy Environ. Sci.*, 2011, **4**, 370–381.
- 46 S. Ardo and G. J. Meyer, *Chem. Soc. Rev.*, 2009, **38**, 115–164.
- 47 J. N. Clifford, E. Palomares, M. K. Nazeeruddin, M. Grätzel and J. R. Durrant, *J. Phys. Chem. C*, 2007, **111**, 6561–6567.
- 48 D. Kuciauskas, M. S. Freund, H. B. Gray, J. R. Winkler and N. S. Lewis, *J. Phys. Chem. B*, 2000, **105**, 392–403.
- 49 S. M. Feldt, G. Wang, G. Boschloo and A. Hagfeldt, *J. Phys. Chem. C*, 2011, **115**, 21500–21507.
- 50 J. P. Hurvois and C. Moinet, *J. Organomet. Chem.*, 2005, **690**, 1829–1839.
- 51 G. Zotti, G. Schiavon, S. Zecchin and D. Favretto, *J. Electroanal. Chem.*, 1998, **456**, 217–221.
- 52 B. A. Gregg, F. Pichot, S. Ferrere and C. L. Fields, *J. Phys. Chem. B*, 2001, **105**, 1422–1429.
- 53 T. W. Hamann, O. K. Farha and J. T. Hupp, *J. Phys. Chem. C*, 2008, **112**, 19756–19764.
- 54 S. M. Waita, B. O. Aduda, J. M. Mwabora, G. A. Niklasson, C. G. Granqvist and G. Boschloo, *J. Electroanal. Chem.*, 2009, **637**, 79–83.
- 55 K. N. Brown, P. T. Gulyas, P. A. Lay, N. S. McAlpine, A. F. Masters and L. Phillips, *J. Chem. Soc., Dalton Trans.*, 1993, 835–840.
- 56 I. Noviandri, K. N. Brown, D. S. Fleming, P. T. Gulyas, P. A. Lay, A. F. Masters and L. Phillips, *J. Phys. Chem. B*, 1999, **103**, 6713–6722.
- 57 V. V. Pavlishchuk and A. W. Addison, *Inorg. Chim. Acta*, 2000, **298**, 97–102.
- 58 P. M. Sommel, B. C. O'Regan, R. R. Haswell, H. J. P. Smit, N. J. Bakker, J. J. T. Smits, J. M. Kroon and J. A. M. van Roosmalen, *J. Phys. Chem. B*, 2006, **110**, 19191–19197.
- 59 N. G. Connelly and W. E. Geiger, *Chem. Rev.*, 1996, **96**, 877–910.
- 60 J. Langmaier, A. Trojánek and Z. Samec, *J. Electroanal. Chem.*, 2008, **616**, 57–63.
- 61 M. A. Bazhenova, S. S. Bogush, A. G. Herbst, T. V. Demeshchik, Y. G. Komarovskaya, V. S. Kurova, M. D. Reshetova, A. D. Ryabov, E. S. Ryabova and Y. N. Frrsova, *Russ. Chem. Bull.*, 1996, **45**, 2445–2451.
- 62 S. K. Sukardi, J. Zhang, I. Burgar, M. D. Horne, A. F. Hollenkamp, D. R. MacFarlane and A. M. Bond, *Electrochem. Commun.*, 2008, **10**, 250–254.
- 63 Y. Wang, E. I. Rogers and R. G. Compton, *J. Electroanal. Chem.*, 2010, **648**, 15–19.
- 64 S. Y. Huang, G. Schlichthorl, A. J. Nozik, M. Grätzel and A. J. Frank, *J. Phys. Chem. B*, 1997, **101**, 2576–2582.
- 65 A. Y. Anderson, P. R. F. Barnes, J. R. Durrant and B. C. O'Regan, *J. Phys. Chem. C*, 2011, **115**, 2439–2447.
- 66 X.-H. Zhang, Y. Cui, R. Katoh, N. Koumura and K. Hara, *J. Phys. Chem. C*, 2010, **114**, 18283–18290.
- 67 U. B. Cappel, S. M. Feldt, J. Schoeneboom, A. Hagfeldt and G. Boschloo, *J. Am. Chem. Soc.*, 2010, **132**, 9096–9101.
- 68 D. R. Lide, *CRC Handbook of Chemistry and Physics – Internet version*, 2005, vol. 85, 6–187; pp. 186–189.
- 69 Y. Liu, J. R. Jennings, M. Parameswaran and Q. Wang, *Energy Environ. Sci.*, 2011, **4**, 564–571.
- 70 L. M. Peter and K. G. U. Wijayantha, *Electrochem. Commun.*, 1999, **1**, 576–580.
- 71 L. M. Peter and K. G. U. Wijayantha, *Electrochim. Acta*, 2000, **45**, 4543–4551.
- 72 N. W. Duffy, L. M. Peter, R. M. G. Rajapakse and K. G. U. Wijayantha, *Electrochem. Commun.*, 2000, **2**, 658–662.